Eur. Phys. J. D **42**, 349–357 (2007)
DOI: 10.1140/epjd/e2007-00008-x

THE EUROPEAN PHYSICAL JOURNAL D

Zonal model of nonstationary self-focusing of femtosecond laser radiation in air: effective beam characteristics evolution

A.A. Zemlyanov and Y.E. Geints[a]

Institute of Atmospheric Optics, Siberian Branch of the Russian Academy of Sciences, Academicheskii ave. 1, 634055 Tomsk, Russia

Received 13 April 2006 / Received in final form 9 October 2006
Published online 17 January 2007 –

Abstract. The generic scenario of intense femtosecond laser pulse propagation in the air from the viewpoint of evolution of its integral effective parameters (energy transfer coefficient, effective radius, effective duration, limiting angular divergence) is considered. The analysis of variation of the effective parameters along the propagation path in the single and multiply filamentation scenarios based on numerical calculations is presented. It is shown that the process of self-action of the ultrashort radiation is characterized by the formation in a medium of the nonlinearity layer, after which optical pulse propagates quasi-linearly with the limiting angular divergence that depends mainly on initial pulse power. The effective pulse temporal duration and the effective beam radius increase after the passage through the nonlinearity layer, and their values are mostly determined by the initial beam power also. The coefficient of energy transmission of femtosecond laser radiation is lower than in the linear medium and has a tendency to decrease with the increase of the pulse power.

PACS. 42.25.Bs Wave propagation, transmission and absorption – 42.68.Ay Propagation, transmission, attenuation, and radiative transfer – 42.65.Jx Beam trapping, self-focusing and defocusing; self-phase modulation

1 Introduction

Propagation of high-power femtosecond laser radiation through gaseous and condensed medium occurs in the nonlinear regime and results in significant changes of temporal, spatial and spectral characteristics of light beam. By now in scientific literature there are numerous discussions concerning the issues of high-power ultrashort radiation propagation through the atmosphere and the prospects of practical applications of nonlinear interaction effects arising during this propagation for the purposes of diagnostic of certain atmospheric parameters [1–8]. High peak power reached in femtosecond pulses determines their propagation in the atmosphere in the mode of self-channeling and strong spatiotemporal phase self-modulation. As a result of dynamic balance between the focusing effect of Kerr nonlinearity and defocusing action of plasma formed in the radiation channel upon a multiphoton ionization of the medium, the beam gets filamented. Thus, the frequency spectrum of optical pulse is highly enriched, and supercontinuum radiation (SC) is formed. The spectral width of this radiation in atmospheric air can be very broad and is comparable with the operating frequency of the initial radiation covering the UV and the near IR regions [3]. With such broadband source it seems realistic to perform simultaneous detection at multiple frequencies of gas and aerosol atmospheric components and atmospheric pollutants also (see, e.g., [5]).

The physical scenarios of filamentation and formation of SC in the atmosphere are the subject of research in many theoretical and experimental papers (their overview can be found, for example, in [9,10]). The experimenters deal, as a rule, with laser beam integral energetic and dimensioning parameters averaged over time and/or space, such as, for example, total pulse energy in the whole spectral interval, transverse fluence distribution, angular divergence, etc. The development of experimental research imposes requirements on theoretical issues as well: demanded are those theoretical models that would be efficient in interpreting experimental data.

It is known that for the stationary self-action of laser radiation the transformation of its energy characteristics can be studied on the basis of effective parameters such as power (energy) transmission coefficient, effective (energy) beam radius, angular divergence, and mean intensity which characterize the global changes of light beam as a whole. In a number of cases, for example, at a stationary self-focusing in Kerr medium [11], at a thermal blooming

[a] e-mail: ygeints@iao.ru

of long laser pulses [12] for some of the effective characteristics one can write a set of differential equations that would adequately describe the quantitative and qualitative sides of the nonlinear propagation process.

For high-power femtosecond radiation that travels in a medium in the non-stationary self-action mode with formation of light and plasma filaments, derivation of such equations for the averaged beam characteristics is yet the problem to be solved in future. The primary method of theoretical research of self-focusing of an ultrashort pulse in a medium is the numerical solution of (3+1)-dimensional vector wave equation for the electric field or its paraxial scalar version known as the nonlinear Schrödinger equation (NLSE) for the optical field envelope coupled with a suitable model for the electron plasma concentration. Nevertheless, the description of the self-focusing phenomenon on basis of effective characteristics of light radiation is productive since it successfully describes the fundamental transformations of a light beam in the nonlinear medium and is capable to forecast the radiation propagation to the distances much exceeding the diffraction length of the beam.

Below we consider the peculiarities in the propagation of a femtosecond laser pulse from the viewpoint of evolution of its effective parameters. Based on the concepts of spatial self-action zones (or, stages) suggested in [13], we present a thorough analysis of the variation of the effective beam parameters along the propagation path, discussing the regimes of a single axial filament formation and multiple filamentation (MF). This enables us to derive analytical expressions for each of the spatial zones thus well approximating the real behavior of the main integral characteristics of laser radiation, namely, the effective radius and the average pulse duration. The input parameters to these relations are the initial pulse radius, the curvature of its phase front, and the duration and peak power of the incident pulse.

2 Research method. Basic approximations

We performed numerical simulation of the self-action of an ultra-short laser pulse in the atmosphere on a horizontal path with no aerosols or turbulence. The ground for numerical calculation of the effective parameters is the nonlinear Schrödinger equation that describes propagation of the electromagnetic wave in a medium in the approximation of a slowly varying field envelope $\mathbf{E}(\mathbf{r}_\perp, z\,; t)$ and is completed with the rate equation for free plasma electron concentration. The complete mathematical formulation of the considered problem can be found elsewhere (for details see, e.g., Refs. [9,14]). The model has been used takes into account transverse diffraction of optical wave in presence of group-velocity dispersion (GVD) up to the second order, as well as the main physical processes governing medium nonlinearity for ultrashort radiation: the instant and time-delayed Kerr effect, nonlinear absorption (MPA) and refraction of radiation by plasma field formed upon multiphoton gas ionization (MPI). We have neglected several high-order nonlinear effects, namely spatiotemporal focusing, self-steepening, and nonlinear dispersion because they do not appear to be key-players in the filamentation process at a moderate input beam power [3]. The model NLSE has the following form:

$$\left\{\frac{\partial}{\partial z} - x\frac{i}{2n_0k_0}\nabla_\perp^2 + i\frac{k''_\omega}{2}\frac{\partial^2}{\partial t^2}\right\}\mathbf{E}(\mathbf{r}_\perp, z\,; t) - ik_0n_2$$
$$\times\left\{(1-f_R)\left|\mathbf{E}\right|^2 + f_R\int\limits_{-\infty}^{\infty} dt'\Lambda(t-t')\left|\mathbf{E}(t')\right|^2\right\}\mathbf{E}(\mathbf{r}_\perp, z; t)$$
$$+\frac{\eta_{cas}}{2}(1+i\omega_0\tau_c)\,\rho_e(\mathbf{r}_\perp, z\,; t)\mathbf{E}(\mathbf{r}_\perp, z\,; t)$$
$$+\frac{\eta^{(K)}_{MPA}}{2}\left|\mathbf{E}\right|^{2K-2}\mathbf{E}(\mathbf{r}_\perp, z\,; t) = 0, \qquad (1)$$

where $|\mathbf{r}_\perp| = \sqrt{x^2+y^2}$, ω_0 is the central frequency of laser radiation; $k_0 = n_0\omega_0/c$ is the wave number; $k''_\omega = \partial^2 k/\partial\omega^2 = 0.21$ fs^2/cm is the group-velocity dispersion in air; $n_2 = 3.2\times10^{-19}$ cm^2/W is the nonlinear part of air refractive index (n_0 is the linear part); f_R is the specific inertial Kerr effect with the response function $\Lambda(t-t')$ (model of a damped oscillator with 20 THz frequency and 70 fs time decay) in the overall change of the nonlinear refractive index (usually assumed $f_R = 0.5$); $\tau_c = 350$ fs is the characteristic time of electronic collision in air; $\eta^{(K)}_{MPA}$ is the K-photon absorption coefficient, and η_{cas} is the cross-section for inverse bremsstrahlung.

The time variation of free electronic concentration ρ_e was calculated according to the equilibrium under-dense plasma model regardless of recombination losses (Drude model [15]):

$$\frac{\partial\rho_e}{\partial t} = \frac{\eta^{(K)}_{MPA}}{K\hbar\omega_0}\left|U\right|^{2K} + \frac{\eta_{cas}}{n_0\Delta E_i}\rho_e\left|U\right|^2, \qquad (2)$$

where $\Delta E_i = 12.1$ eV is the ionization potential of oxygen atom. For multiphoton ionization of oxygen $K = 8$ photons can liberate an electron at a laser wavelength of $\lambda_0 = 800$ nm. The absorption K-photon coefficient $\eta^{(K)}_{MPA}$ is obtained from the experimental data [16] and equals $\eta^{(K)}_{MPA} = 3.6\times10^{-121}$ m^{13} W^{-7}. Plasma cross-section for the inverse bremsstrahlung η_{cas} is calculated in the framework of the Drude model and reads $\eta_{cas} = 5.1\times10^{-22}$ m^2.

In the numerical simulation, the Gaussian spatiotemporal laser pulse profile is used as a set of initial condition:

$$\mathbf{E}(\mathbf{r}_\perp z = 0; t) = \exp\left\{-\frac{\mathbf{r}_\perp^2}{2R_0^2}\left(1+\frac{ik_0R_0^2}{F}\right)\right\}\exp\left\{-\frac{t^2}{2t_p^2}\right\}, \qquad (3)$$

where $k_0 = 2\pi/\lambda_0$ is the module of the wave vector at pulse central wavelength $\lambda_0 = 810$ nm, $t_p = 80$ fs is pulse duration ($1/e$ temporal width), $R_0 = 1$ mm is laser beam waist. The initial phase front curvature radius F is chosen to be equal to double beam Rayleigh length: $L_R = k_0R_0^2/2$, so that $F = 2L_R$. Later on, for convenience, we will consider the normalized variables: $\mathbf{r}_\perp/R_0$, z/L_R, F/L_R, t/t_p.

The numerical integration of NLSE was performed by means of original problem splitting into two subproblems: the nonlinear one where the field nonlinear phase formation is calculated, and the linear one where the field amplitude is transformed due to free space diffraction and chromatic dispersion of the wavelet with the phase front determined at the preceding step (see, e.g., Ref. [4]). To improve the calculation reliability, we used the combination of the spectral Fourier method (along temporal pulse dimension), the implicit three-layer Crank-Nicholson scheme (along transverse coordinates), and the adaptive mesh (along the evolutionary variable). The limiting resolution of the computational grid was ∼20 μm in transverse direction and ∼3 fs in time, which was sufficient to simulate the basic physical engines of self-action of laser radiation in air. To raise the calculation speed, formation of a single axial light filament in air was modeled by means of the reduced axisymmetric (2D+1) version of NLSE (in cylindrical coordinates the transverse divergence operator is expressed as: $\nabla_\perp^2 = (1/r)\partial/\partial r + \partial^2/\partial r^2$). The MF regime was modeled by solving the full (3D+1) NLSE. In transverse direction, calculation grid domain equals $35R_0$ for the axisymmetric NLSE and $15R_0$ for the calculations in the Cartesian coordinate system. This ensured no artifacts in the transverse distribution of field amplitude due to reflection of the numerical scheme from grid domain boundaries.

The effective laser pulse parameters are calculated as the second order integral moments based on computed local field characteristics (optical field envelope, spectral and spatial energy density) according the equations presented in [13] and below in Section 3 of this paper.

3 Effective (integral) characteristics of optical pulse

The classical definition [11] states that the effective (generalized) light beam parameters are integral functionals of the optical field intensity $I(\mathbf{r}_\perp, z; t) = (cn_0/8\pi)\left|\mathbf{E}(\mathbf{r}_\perp, z; t)\right|^2$ at every space point $(\mathbf{r}_\perp, z)$ and at every time moment t. Hence, there follows the squared effective beam energy radius (waist) R_e:

$$R_e^2(z) = \frac{1}{E(z)} \int\limits_{-\infty}^{\infty} dt' \iint\limits_{\mathbf{R}_\perp} d^2\mathbf{r}_\perp I(\mathbf{r}_\perp, z; t') \left|(\mathbf{r}_\perp - \mathbf{r}_{gr})\right|^2 \tag{4}$$

where $E(z) = \int\limits_{-\infty}^{\infty} dt' \iint\limits_{\mathbf{R}_\perp} d^2\mathbf{r}_\perp I(\mathbf{r}_\perp, z; t')$ stands for the total energy of the optical pulse along the propagation path, $\mathbf{r}_{gr}(z) = [1/E(z)] \int\limits_{-\infty}^{\infty} dt' \iint\limits_{\mathbf{R}_\perp} d^2\mathbf{r}_\perp \left[\mathbf{r}_\perp I(\mathbf{r}_\perp, z; t')\right]$ is the radius-vector of the beam gravity centre.

The squared effective pulse temporal duration t_{pe} has a similar form:

$$t_{pe}^2(z) = \frac{1}{E(z)} \iint\limits_{\mathbf{R}_\perp} d^2\mathbf{r}_\perp \int\limits_{-\infty}^{\infty} dt' I(\mathbf{r}_\perp, z; t') \left(t' - t_0\right)^2, \tag{5}$$

where $t_0(z) = [1/E(z)] \iint\limits_{\mathbf{R}_\perp} d^2\mathbf{r}_\perp \int\limits_{-\infty}^{\infty} dt' \left[t' I(\mathbf{r}_\perp, z; t')\right]$ is pulse temporal "gravity centre".

Let us introduce the parameter of the limiting effective pulse angular divergence θ_∞, i.e. the divergence the beam possesses in the far-field (diffraction) zone. This parameter is expressed in radians and is determined by the spatial spectrum of the optical wave $\mathbf{S}(\mathbf{k}_\perp, z; t)$, $\mathbf{k}_\perp \in \mathbf{K}_\perp$, as follows:

$$\theta_\infty = \frac{\lambda_0}{2\pi} \lim_{z\to\infty} \left[\frac{1}{E(z)} \int\limits_{-\infty}^{\infty} dt' \times \iint\limits_{\mathbf{K}_\perp} d^2\mathbf{k}_\perp \left|\mathbf{S}(\mathbf{k}_\perp, z; t')\right|^2 \left|(\mathbf{k}_\perp - \mathbf{k}_{gr})\right|^2 \right]^{1/2}. \tag{6}$$

Here, λ_0 is operating wavelength, $\mathbf{k}_\perp = (k_x, k_y) = 2\pi/\mathbf{r}_\perp$ is transversal component of wave vector, $[\mathbf{k}_{gr}(z)\lambda_0/2\pi]$ is the global angular shift of beam axis.

Another important integral parameter of the laser pulse is the energy transfer coefficient T_e that characterizes energy losses after the beam passes the distance z:

$$T_e(z) = E(z)/E_0, \tag{7}$$

where E_0 is total energy of incident optical pulse.

And finally, the spectral composition of the optical pulse will be characterized by the average (over beam cross-section) effective spectral width Δ_ω, whose square is found similarly to equation (5):

$$\Delta_\omega^2(z) = \frac{1}{E(z)} \iint\limits_{\mathbf{R}_\perp} d^2\mathbf{r}_\perp \int\limits_{-\infty}^{\infty} d\omega \left|\mathbf{F}(\mathbf{r}_\perp, z; \omega)\right|^2 \left(\omega - \omega_{gr}\right)^2, \tag{8}$$

where $\omega_{gr}(z) = [1/E(z)] \iint\limits_{\mathbf{R}_\perp} d^2\mathbf{r}_\perp \int\limits_{-\infty}^{\infty} d\omega \left|\mathbf{F}(\mathbf{r}_\perp, z; \omega)\right|^2 \omega$ is the position of the gravity centre of the pulse frequency spectrum, and $\mathbf{F}(\mathbf{r}_\perp, z; \omega)$ is the frequency Fourier transform of the electric field $\mathbf{E}(\mathbf{r}_\perp, z; t)$.

As will be seen below, the effective beam parameters are an efficient tool in the description and analysis of radiation transformation in a non-linear medium. In principle, at each point on the propagation path, the effective parameters calculated according to equations (4)–(8) can be applied to an ideal-shaped Gaussian spatiotemporal profile embedded into the original pulse intensity distribution and having the radius $R_e(z)$, the characteristic pulse duration $t_{pe}(z)$ and the effective peak intensity $I_e(z) = E(z)/\left[\pi^{3/2} R_e^2(z) t_{pe}(z)\right]$.

Now, using the introduced effective beam characteristics equations (4)–(8), we will trace the evolution and analyze the main phases of the nonstationary self-focusing of a femtosecond laser pulse in the atmospheric air.

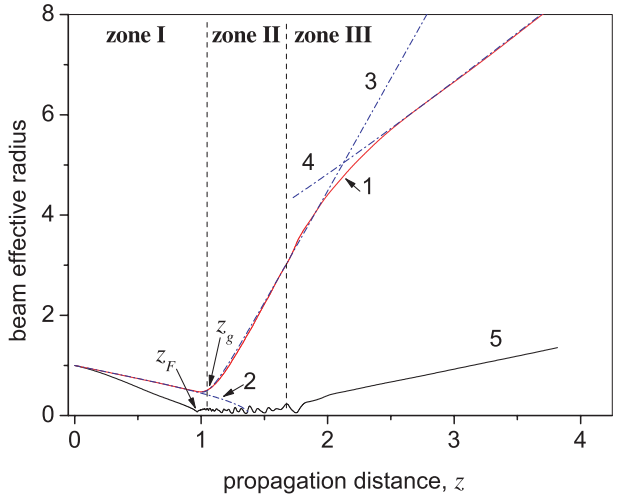

Fig. 1. (Color online) The evolution along the optical path of normalized effective beam radius $\bar{R}_e = R_e/R_0$ (curve 1) and the radius determined by e^{-1} level in the fluence profile $\bar{R} = R/R_0$ (curve 5), at femtosecond pulse filamentation in air. A conditional division into evolution zones of $R_e(z)$, local and global beam nonlinear foci are illustrated. Curves 2, 3, and 4 are plotted according to equations (9) and (11). The initial pulse power equals to $\eta = 2$.

4 Evolution of laser pulse effective parameters at a nonstationary self-action in air

In a nondissipative Kerr medium in the absence of chromatic dispersion and nonlinear beam aberrations, the characteristics T_e, t_{pe} are invariants along z-axis up to the nonlinear focus, which shows the quadratic dependence of the effective radius R_e along the longitudinal coordinate [11]. Self-focusing of the ultrashort radiation in a medium leads to regions of high laser intensity where multiphoton ionization produces plasma. Plasma electrons cause the nonlinear absorption of the optical wave and its defocusing. A simultaneous manifestation of Kerr focusing and plasma defocusing effects leads to a strong phase self-modulation of radiation, and thus, the parameters T_e and t_{pe} lose their invariance property.

Figures 1 and 2 show evolution of the effective pulse parameters along the propagation path in air. From Figure 1 follows that the behavior of function $R_e(z)$ allows one to mark out three spatial zones (as is shown in the figure), each having a dominant physical process governing the global dynamics of the effective radiation parameters.

At the beginning of the self-focusing, i.e. in the *Zone I*, the beam is transversely compressed due to Kerr effect. The growth of the peak pulse intensity and the subsequent multiphoton absorption yield medium ionization and plasma generation. The defocusing effect of the generated plasma channel and the light energy losses both arrest beam collapse and lead to the formation at $z_F \approx 0.97$ (for $\eta = P_0/P_c = 2$, where $P_c = \lambda_0^2/2\pi n_2 = 3.2$ GW is the critical self-focusing power in air) on the beam axis of a waveguide channel — a light filament. This filament

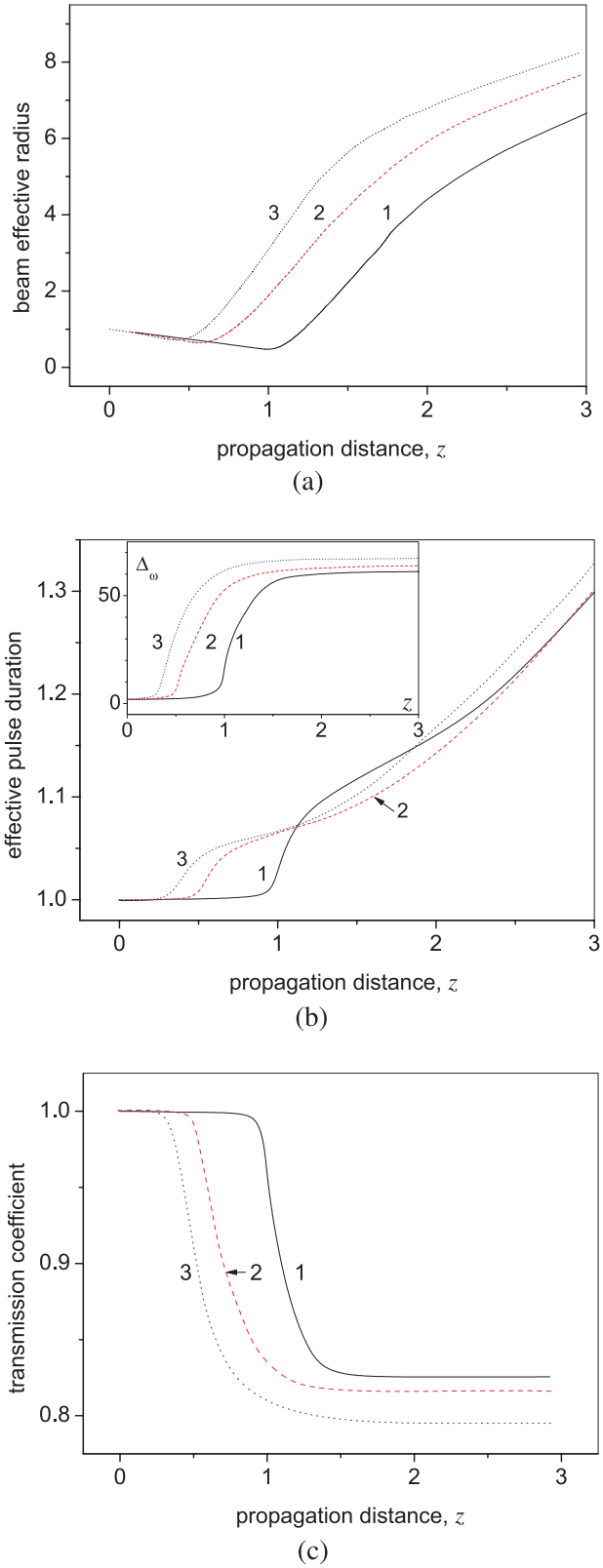

Fig. 2. (Color online) Effective radius $\bar{R}_e$ (a), effective pulse duration $\bar{t}_{pe} = t_{pe}/t_p$ (b), average frequency spectrum width $\bar{\Delta}_\omega = \Delta_\omega(z)/\Delta_\omega(0)$ (the inset), beam energy transmission coefficient T_e (c) along the propagation path in air at different initial peak powers: $\eta = 2$ (curve 1); 5 (curve 2); 10 (curve 3). All values are normalized to those at path starting point.

has a pulsed transverse size and a nearly zero angular divergence. The transverse filament size in air varies from 75 to 150 μm at filament peak intensity of $\sim 10^{14}$ W/cm^2. The maximal density of free electrons in plasma channel can reach 10^{21}–10^{23} m^{-3}. Filament formation does not restrain transverse compression of the beam as a whole, therefore the "global" nonlinear focus z_g determined by the minimum value of R_e is located to the right (along z-axis) of the local nonlinear focus z_F.

This spatial zone, almost up to the global nonlinear focus, as follows from Figure 3a, features sharpening of the Gaussian fluence spatial profile of the laser pulse. The magnitude and width of beam transverse intensity distribution vary due to beam self-focusing in a cubic nonlinear medium. The total beam energy E in this zone to the first approximation can be considered constant and equal to the initial energy E_0. The GVD effects in this zone are negligible too. Hence, to approximate the function $R_e(z)$ in *Zone I* it is possible to use well-known theory of Kerr self-focusing [11] and write down the following relation:

$$R_e^2(z) = R_{e0}^2 \left[(1-\eta*) \left(\frac{z}{2}\right)^2 + \left(1 - \frac{z}{F}\right)^2 \right] = R_{e0}^2 \left[\theta_I^2 \left(\frac{z}{2}\right)^2 - 2\frac{z}{F} \right], \qquad z \in [0; z_g]. \quad (9)$$

Here $R_{e0} \equiv R_e(z = 0) = R_0$; $\eta* = P_0/P_c^*$; $\theta_I = \sqrt{|(1-\eta*)| + 4/F^2}$ is beam angular divergence (in *Zone I*) normalized to the initial diffraction-limited divergence of collimated beam: $\theta_D = 1/(k_0 R_0)$, P_0 is the pulse peak power as it enters the medium, and $P_c^* = bP_c$ is the effective critical self-focusing power determined with regard to the combined (instant and time-delayed response) Kerr nonlinearity and differs from its standard value by the coefficient $b \approx 1.62$. We note that this coefficient is obtained by approximating numerical data according to equation (9) and does not depend on the initial pulse power. The analytical estimate of the effective critical beam power can be found in references [17,18].

Surprisingly, the position of "global" nonlinear focus z_g closely agrees with the value obtained according to equation (9) by evaluating the condition $R_e(z_g) = 0$ with the parameter $\eta* = \eta$:

$$z_g = \frac{F}{\sqrt{\eta - 1}\,(F/2) + 1}. \quad (10)$$

The following zone (*Zone II*) we have marked out with respect to the evolution of the effective beam parameters is characterized by their most dynamic longitudinal changes. An active multiphoton ionization of the medium significantly decreases the total beam energy (see Fig. 2c). Also, the temporal pulse profile breaks into a sequence of short spikes, each of $t_{pN} \sim 0.1 t_p$ duration which significantly enhances the role of medium chromatic dispersion in the whole process of phase self-modulation. As a result, the pulse temporally been Gaussian at the starting point transforms into a sequence of "pulselets" separated in time and space. These pulselets undergo much stronger GVD than the original pulse does, and pulse average duration

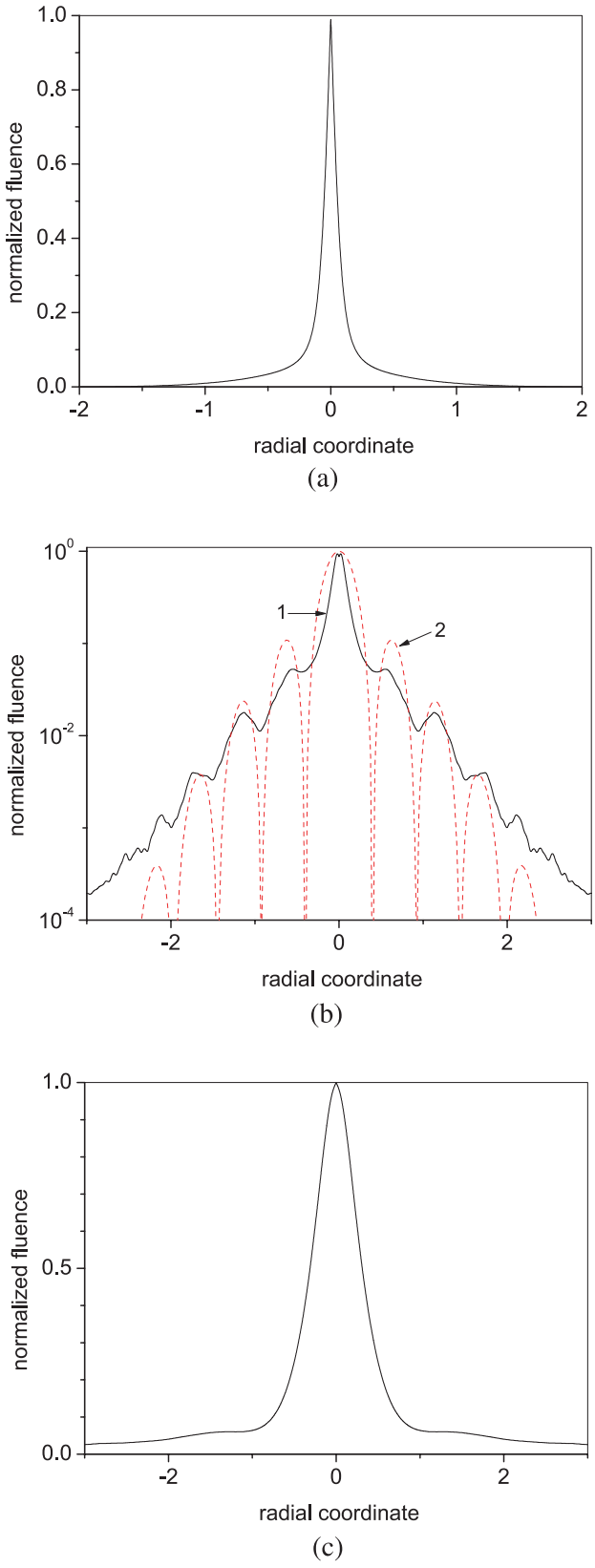

Fig. 3. Transverse beam fluence profile (normalized to its maximal value) at different distances along the propagation path: $z = 0.4$ (a), 0.7 (b), and 2.0 (c). In (b) the real profile and its approximation by equation (11) are shown by curves 1 and 2 respectively. Pulse initial peak power corresponds to $\eta = 7$.

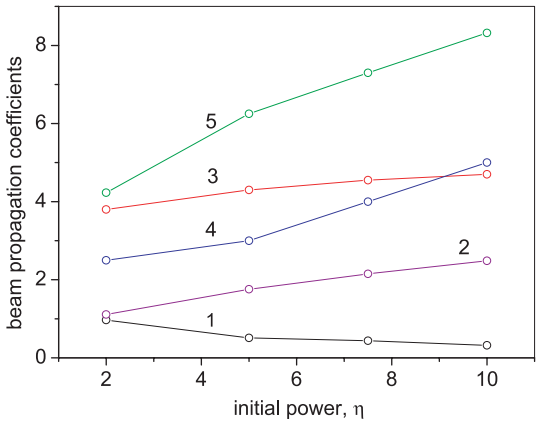

Fig. 4. (Color online) The coordinate of global nonlinear beam focus z_g in *Zone I* (curve 1); normalized angular divergence in *Zone I* θ_I (curve 2), normalized to θ_D limiting angular divergence in *Zone III* $\bar{\theta}_\infty$ (curve 3), normalized effective radius at the end of *Zone II* $\bar{R}_{eL}$ (curve 4), and propagation coefficient in *Zone II* M^2 (curve 5), depending on the pulse power parameter η. For pictorial indication the numerical results shown by points are connected by straight lines.

t_{pe} rises stepwise and then gradually increases with the distance (see Fig. 2b). Temporal pulse breakup together with plasma formation enrich laser pulse frequency spectrum that leads to the strong increase of pulse average spectral width Δ_ω (see the inset in Fig. 2b).

The behavior of the effective beam radius $R_e(z)$ in this spatial zone resembles its evolution behind focal waist at beam free diffraction in vacuum. In this case, for beams with axially symmetrical spatial profile, the law of longitudinal variation of the effective radius takes the known form [11]:

$$R_e^2(z) = R_{ew}^2 \left[1 + \theta_{II}^2 \frac{(z - z_w)^2}{4}\right], \qquad (11)$$

where $R_{ew} \equiv R_e(z = z_w)$ is the effective beam waist located at z_w; $\theta_{II} = M^2 R_{e0}/R_{ew}$ is the normalized to θ_D angular divergence (in *Zone II*); $M^2 \geqslant 1$ is the so-called beam propagation coefficient [19]. The lowest value of this coefficient complies with the Gaussian beam ($M^2 = 1$), hence, the factor M^2 is often referred to as beam quality criterion. The larger is the value of M^2, the stronger is the distinction of the transverse intensity profile from Gaussian shape.

Our calculations show that the approximation of the function $R_e(z)$ in *Zone II* by equation (11) in the range $z \geqslant z_g$ gives a pronounced dependence of M^2 on the initial pulse power, characterized by the dimensionless parameter η. This dependence is close to linear one and is illustrated in Figure 4. The fact that M^2 has values greater than unity, points out non-Gaussian fluence distribution of laser pulse, which can also be seen in Figure 3.

Indeed, in the filamentation zone, beam spatial profile has the form of a central peak encircled by a system of concentric rings (Fig. 3b) formed upon the interference of counter-propagated energy fluxes from beam periphery to its centre and vice versa in successive refocusing events of pulse time slices. The Bessel-Gaussian (BG) beam profile is closest to such a distribution; and it is set by the cylindrical Bessel function $J_0(r)$ bounded by the Gaussian aperture r_g:

$$U(r) \propto J_0(\beta_0 r) \exp\left(-r^2/r_g^2\right), \qquad (12)$$

where $\beta_0 \geqslant 1$ is the parameter responsible for the number of rings. As known [20], diffraction of such beams is very special; it starts from beam periphery and the radius of the axial peak remains nearly unchanged over the distance $L_{BG} = kr_g^2/2\beta_0$, while the propagation coefficient $M_{BG}^2 = \left\{[1 + \mu I_1(\mu)/I_0(\mu)]^2 - \mu^2\right\}^{1/2}$ (where $\mu = (\beta_0 r_g)^2/4$, $I_{0,1}(\mu)$ are the modified Bessel functions) far exceeds unity.

Within the concepts of the BG beam diffraction, the growth of the coefficient M^2 with the increase in power P_0 at a self-action of ultrashort radiation can be explained easily. The growth in η increases the number of optical field refocusing events on beam axis approximately by $\sim\eta/2$. In its turn, this increases the number of interference rings in beam profile, which corresponds to the growth of the parameter β_0, shortening of Rayleigh distance L_{BG}, and the growth in the angular beam divergence.

With a further propagation of the laser pulse in a medium, beam modulation instability together with dispersion-induced blur effect and the energy spent on plasma formation, break the conditions of self-channeling and the light filament stops its existence. From this moment on, diffraction-induced beam spreading prevails over Kerr focusing, which makes the rings in the transverse fluence profile fade and finally vanish (see Fig. 3c). Simultaneously, the effective beam radius growth rates and its angular divergence decrease. Now, from this point on the evolution of the effective beam parameters enters spatial *Zone III*.

In this spatial region the dependence $R_e^2(z)$ can again be described by a quadratic law (see, Eq. (11)) with the limiting angular divergence θ_∞ and the beam effective waist $R_{eL} \equiv R_e(z = z_L)$, where z_L is the boundary coordinate between *Zone II* and *Zone III*. Actually, z_L is a conditional boundary of the nonlinear medium layer, behind which the evolution of effective beam parameters obeys the linear diffraction laws. The transverse beam fluence profile in *Zone III*, as is seen from Figure 3d, resumes a smooth near-Lorentzian shape.

The values of $\bar{R}_{eL} = R_{eL}/R_0$ and $\bar{\theta}_\infty = \theta_\infty/\theta_D$ obtained from numerical calculations for different values of initial pulse power are shown in Figure 4. We note the tendency of a gradual growth of beam limiting divergence with the increase of pulse power in the linear diffraction zone (*Zone III*). A similar dependence possesses the effective beam waist R_{eL}. Note, that for both considered spatial domains (*Zone II* and *Zone III*) a slight growth of the global angular divergence with the increase in the pulse input power is observed which indicates the increase in nonlinear Kerr-lens strength formed in the medium upon pulse self-focusing.

Our calculations show that the variation with z of effective pulse duration t_{pe} (as seen from Fig. 2b) in *Zones II* and *III* is well described by the linear propagation law of a short pulse in a medium with normal-type GVD:

$$t_{pe}(z) = t_{pe}(z_g)\sqrt{1 + [(z - z_g)/L_{dsN}]^2}; \quad z \geqslant z_g. \quad (13)$$

The effective pulse duration variation is characterized by a new dispersion length L_{dsN}, that only weakly depends on beam power P_0. Here, the following relation between the original $L_{ds} = t_p^2/k''$ and the newly introduced dispersion lengths is valid: $L_{ds}/L_{dsN} = (t_p/t_{pN})^2 \approx 10^2$. The magnitude of the step in $t_{pe}(z_g)$ dependence at the beginning of *Zone II* weakly depends on P_0 also.

The beam energy transfer coefficient T_e versus z at various initial radiation powers is shown in Figure 2c, therefrom we see that for high-power beams, the nonlinear energy losses becomes essential and to the end of the optical path can achieve ∼20% of the initial pulse energy. The main reason for light energy dissipation is MPA process in air that forms a plasma column on the beam axis. Thus, all relevant energy losses occur in *Zone II* as long as the filament exists. Violation of the dynamic balance between Kerr and plasma nonlinearities breaks up the filament, stops medium ionization, and stabilizes the energy transfer coefficient T_e.

5 Effective parameters evolution during MF scenario

Below we will focus on the situation, when self-action of femtosecond radiation produces several filaments instead of single one. The numerical calculations reported above in this paper were performed for the beam with the ideal Gaussian spatial profile with no turbulence in a medium. In this case, at a self-focusing, the peak intensity is always located on beam axis resulting in only one axial filament. The non-Gaussian fluence profile (e.g., super-Gaussian, or spiking shape) as well as perturbations in the amplitude and/or phase of the optical wave that arise, for instance, because of nonideality of the optical system forming the beam and the influence of turbulent fluctuations of medium refraction index, in real situations yield randomly organized multiple filamentation (MF) over the whole beam cross-section. Namely, the higher is the beam power, the stronger and more complicated are filamentation patterns [14,18,21–23]. It was established that each separate light filament possesses roughly a critical power P_c. The filaments themselves are as a rule randomly arranged over the beam cross-section and have different spatial lengths. In the course of their development, filaments can interact, fusing with each other or, on the contrary, breaking down to shorter fractions.

It seems likely that such complex filamentation dynamics of high-power beams must affect their effective parameters. To properly model the MF regime we have performed the numerical solution of NLSE for the light beam, whose transverse profile differs from the ideal Gaussian shape

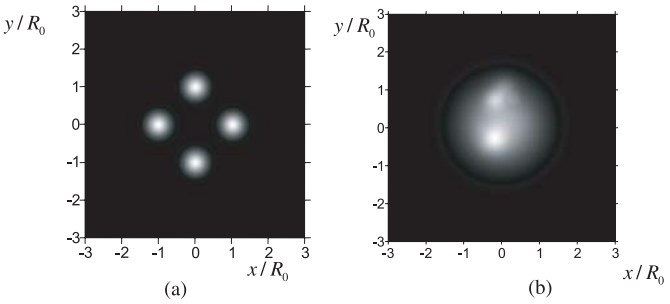

Fig. 5. Transverse beam fluence profiles used in numerical calculations of pulse self-focusing in MF regime ($r_0 = R_0$, $N_p = 4$): (a) according to equation (14); (b) according to equation (15).

and has (1) a coronal structure joining N_p isolated Gaussian peaks positioned equidistantly in circumference of the radius r_0 (see Fig. 5a)

$$\mathbf{E}(x, y, z = 0) \propto \sum_{m=1}^{N_p} \exp\left\{-\frac{(x - x_m)^2 + (y - y_m)^2}{2R_p^2}\right\},$$
$$x_m = r_0 \cos\left(\frac{2\pi m}{N_p}\right),$$
$$y_m = r_0 \sin\left(\frac{2\pi m}{N_p}\right), \quad m = 1 \ldots N_p, \quad (14)$$

where R_p is the width of a single peak, and (2) the Gaussian bell-shaped distribution superimposed by N_p random peaks (see Fig. 5b), that is similar to the beam distribution which filamentation scenario in air was extensively studied in references [14,18]:

$$\mathbf{E}_\perp(x, y, z = 0) \propto \exp\left\{-\frac{(x^2 + y^2)}{2R_0^2}\right\}$$
$$\times \sum_{m=1}^{N_p} \tilde{A}_m \exp\left\{-\frac{(x - \tilde{x}_m)^2 + (y - \tilde{y}_m)^2}{2\tilde{R}_p^2}\right\},$$
$$m = 1 \ldots N_p, \quad (15)$$

where the amplitudes $\tilde{A}_m$, the half-widths $\tilde{R}_p$, and the coordinates of peak centers $(\tilde{x}_m, \tilde{y}_m)$ are normally distributed random numbers. Each of these peaks forms its own filament upon beam self-focusing, but they develop together and interact in a common photon reservoir (the possibility of obtaining regular and controllable MF patterns was recently demonstrated in Ref. [23]).

Figure 6 depicts spatial dynamics of the effective radius of laser beam with unimodal Gaussian shape and that of the beams with a multiple peak structures equations (14), (15). The peak effective initial power P_{e0}, defined as $P_{e0} = E_0/(\pi^{1/2} t_p)$, the beam waist, and pulse duration in all cases are taken the same. It can be seen that according to the zonal concept of effective beam radius evolution, different scenarios of MF can be developed. Indeed, for the transverse coronal profile (Fig. 5a) there is no remarkable boundary between the second and the

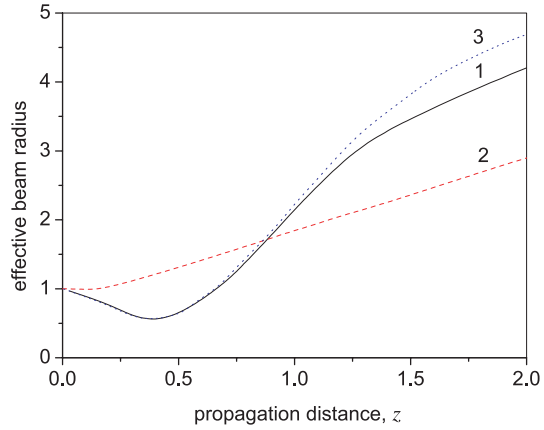

Fig. 6. (Color online) Normalized effective beam radius upon pulse self-focusing under single (curve 1) and multiple (curves 2 and 3) filamentation scenarios with the fluence profile specified by Figure 5a (curve 2), and Figure 5b (curve 3). Initial pulse parameters correspond to $\eta = 10$ and $F = 1$.

third zones, contrary to the case of an ideal Gaussian profile (Fig. 6, curve 2).

Besides, in *Zone I* there is no pulse effective waist reduction due to its self-focusing, probably, because each filament develops within its local vicinity, and there is no tendency of optical field contracting to the beam geometrical axis ($|\mathbf{r}_\perp| = 0$) due to Kerr effect. At the same time in *Zone III* the beam angular divergence under MF is the same as that of the ideal Gaussian beam when a single axial filament forms up. This fact points out to the generic spatial intensity profiles in the linear diffraction zone realized in these two cases. Variation along z of other effective parameters under MF scenario (not shown here) only slightly differs from the considered above regularities in single filamentation regime.

When the initial transverse fluence distribution has a pronounced central peak (Fig. 5b), the evolution of its effective radius under MF scenario is roughly the same as under single filamentation (see Fig. 6, curve 3). This concerns both the transverse beam waist position in *Zone I*, the location of global nonlinear focus and the spreading rate in linear diffraction zone. The results presented show that upon beam self-focusing the low intensity central peak dominates the dynamics of the more intense spikes. More or less discernable distinctions can be seen only in the second spatial zone (*Zone II*) and consist in a faster transverse growth of the beam effective radius and, therefore, its larger effective diameter in *Zone III*.

Thus, we may infer that on the whole, the relative similarity in evolution of the effective parameters of light beams under single and multiple filamentation can be found only behind the nonlinear medium layer, when the filament structure breaks down. Other spatial zones exhibit only a partial similarity in beam effective parameters evolution.

6 Conclusion

In conclusion, self-action of ultrashort laser pulses in the atmospheric air is affected by a large number of physical factors determining the propagation of laser radiation and dynamically balancing each other. The filamentation scenario of the femtosecond pulse is very complex and depends on the light beam initial morphology (spatial and temporal shapes). So, the correct description of pulse dynamics requires the knowledge of the spatiotemporal distribution of the complex field envelope at every point on the propagation path. The use of the effective beam parameters defined as the second order normalized moments of beam energy characteristics, gives a useful overview of the regularities of high-power light energy transfer at its nonstationary self-action in a medium. Here, a real spatiotemporal beam profile can be treated as an ideal-shaped Gaussian (in time and space) profile embedded into the incident field distribution, which allows describing the nonstationary self-action of real beam by applying the well-known self-focusing theory for this model beam, and the linear relations governing the diffraction and propagation of waves through a non-aberrational lens.

In this paper, on the basis of a numerical solution of the nonlinear Schrödinger equation we have considered the regularities of evolution of effective parameters of femtosecond laser pulse upon single and multiple filamentation in air. We have demonstrated that based on the effective parameters evolution along the optical path, it is possible to allocate three spatial zones reflecting different stages of the nonstationary pulse self-focusing, namely: (1) the zone of beam compression toward the global nonlinear focus and filament formation around it; (2) the zone of a sharp increase of the effective beam cross-section behind the nonlinear focus, and (3) the zone of free diffraction of the radiation reformatted by a nonlinear Kerr-lens. For each of these zones, there exist simple analytical relations well describing the real dependence of several effective radiation characteristics on the evolutional variable. The input parameters to these relations are the initial beam radius, its phase front curvature, the duration, and peak power of the original pulse.

In contrast to the case of a single axial filament the MF scenario most strongly affects the evolution of the effective beam radius resulting in a shift of zonal boundaries, though the behavior of other integral beam characteristics remains practically unaffected.

References

1. B. La Fontaine, F. Vidal, Z. Jiang, C.Y. Chien, D. Comtois, A. Desparois, T.W. Johnston, J.-C. Kieffer, H. Pepin, H.P. Mercure, Phys. Plasmas **6**, 1615 (1999)
2. J. Kasparian, R. Sauerbrey, D. Mondelain, S. Niedermeier, J. Yu, J.-P. Wolf, J.-B. Andre, M. Franco, B. Prade, S. Tzortzakis, A. Mysyrowicz, M. Rodriguez, H. Wille, L. Wöste, Opt. Lett. **25**, 1397 (2000)
3. N. Aközbek, M. Scalora, C.M. Bowden, S.L. Chin, Opt. Commun. **191**, 353 (2001)

4. A. Couairon, S. Tzortzakis, L. Berge, M. Franko, B. Prade, A. Mysyrowicz, J. Opt. Soc. Am. B **19**, 1117 (2002)
5. G. Méjean, J. Kasparian, J. Yu, S. Frey, E. Salmon, J.-P. Wolf, Appl. Phys. B **78**, 535 (2004)
6. V.P. Kandidov, I.S. Golubtsov, O.G. Kosareva, Quantum Electron. **34**, 348 (2004)
7. M. Rodriguez, R. Bourayou, G. Méjean, J. Kasparian, J. Yu, E. Salmon, A. Scholz, B. Stecklum, J. Eislöffel, U. Laux, A.P. Hatzes, R. Sauerbrey, L. Wöste, J.-P. Wolf, Phys. Rev. E **69**, 036607 (2004)
8. R. Nuter, L. Bergé, J. Opt. Soc. Am. B **23**, 874 (2006)
9. V.P. Kandidov, O.G. Kosareva, I.S. Golubtsov, W. Liu, A. Becker, N. Aközbek, C.M. Bowden, S.L. Chin, Appl. Phys. B **77**, 149 (2003)
10. P. Sprangle, J.R. Penano, B. Hafizi, Phys. Rev. E **66**, 046418 (2002)
11. S.N. Vlasov, V.A. Petrishchev, V.I. Talanov, Radiophys. Quant. Electron. **14**, 1353 (1971)
12. V.E. Zuev, A.A. Zemlyanov, Yu.D. Kopytin, A.V. Kuzikovskii, *High-power laser radiation in atmospheric aerosols* (Dordrecht, Holland, D. Reidel Publ. Corp., 1984)
13. A.A. Zemlyanov, Yu.E. Geints, Atmos. Oceanic Opt. **18**, 574 (2005)
14. M. Mlejnek, M. Kolesik, J.V. Moloney, E.M. Wright, Phys. Rev. Lett. **83**, 2938 (1999)
15. E. Yablonovitch, N. Bloembergen, Phys. Rev. Lett. **29**, 907 (1972)
16. A. Talebpour, S. Petit, S.L. Chin, Opt. Commun. **171**, 285 (1999)
17. A. Couairon, Eur. Phys. J. D **27**, 159 (2003)
18. O.G. Kosareva, N.A. Panov, N. Akozbek, V.P. Kandidov, Q. Luo, S.A. Hosseini, W. Liu, J.-F. Gravel, G. Roy, S.L. Chin, Appl. Phys. B **82**, 111 (2006)
19. A.E. Siegman, *Lasers* (Oxford University Press, Mill Valley, CA, 1986)
20. F. Gori, G. Guattari, C. Padovani, Opt. Commun. **64**, 491 (1987)
21. W. Liu, S.A. Hosseini, Q. Luo, B. Ferland, S.L. Chin, O.G. Kosareva, N.A. Panov, V.P. Kandidov, New J. Phys. **6**, 1 (2003)
22. G. Méchain, A. Couairon, Y.-B. Andre, C. D'Amico, M. Franko, B. Prade, S. Tzortzakis, A. Mysyrowicz, A. Sauerbrey, Appl. Phys. B **79**, 379 (2004)
23. G. Méchain, A. Couairon, M. Franko, B. Prade, A. Mysyrowicz, Phys. Rev. Lett. **93**, 035003 (2004)